Wear and Corrosion Behavior of Aluminate- and Phosphate-Based Plasma Electrolytic Oxidation Coatings with Polytetrafluoroethylene Nanoparticles on AZ80 Mg Alloy

Ebrahim Mortezanejad, Masoud Atapour, Hamidreza Salimijazi, Amir Alhaji, and Amin Hakimizad

The wear and corrosion behavior of PTFE-containing PEO nanocomposite coatings on AZ80 magnesium alloy were investigated. PEO nanocomposite coatings were produced using aluminate- and phosphate-based electrolytes for 10 min. It was found that PTFE nanoparticles effectively seal the micropores in both aluminate- and phosphate-based coatings. The wear examinations were performed using pin-on-disk (AISI 52100) tests under 2 loads of 3 and 5 N at a distance of 500 m. Compared to the uncoated base metal, the wear rate and the friction coefficient of the nanocomposite coatings with PTFE particles were significantly decreased. Among the prepared coatings, the coating formed in aluminate electrolyte with PTFE nanoparticles exhibited the best wear resistance. The polarization tests revealed that the corrosion resistance of the PTFE-containing coatings was superior to the coatings without PTFE. The coating obtained in the phosphate electrolyte containing PTFE nanoparticles showed the best corrosion performance. These results were confirmed by electrochemical impedance spectroscopy (EIS) and immersion tests for different times of 4, 24, 48 and 72 h immersion in 0.5 wt.% NaCl.

1. Introduction

Magnesium alloys have attracted great interest in different applications due to their high specific strength, good castability and biocompatibility (Ref 1-3). These properties make it valuable in a number of applications including automobile and computer parts, mobile phones, sporting goods, handheld tools and household equipment (Ref 4-6). However, poor corrosion and wear resistance are two major limitations of Mg alloys for further use in different industries (Ref 7-9). Therefore, two strategic methods of alloying and surface modification are seeking the attention of the researchers to enhance the corrosion and wear behavior of Mg alloys (Ref 10, 11). In recent years, the use of plasma electrolytic oxidation (PEO) has gained more and more interest for producing a protective coating on Mg alloys against corrosion and wear (Ref 10, 12). This method can provide functional properties such as reducing friction coefficient, thermal resistance, optical and dielectric properties for a metal or alloy surface (Ref 13). The PEO process is similar to the conventional anodizing, except that it is accomplished at much higher voltages (400-700 V), producing short-term evacuation microchannels (Ref 14, 15). Also, the coatings produced by PEO method have higher hardness and thickness (Ref 15).

Recently, many studies have been carried out to determine the relationship between the structure and properties of the PEO coatings on magnesium alloys in silicate, phosphate and aluminate electrolytes (Ref 16-18). However, it is relatively rare for PEO treatment of Mg alloys in aluminate-based electrolyte (Ref 19). The addition of particles into the PEO electrolyte is a new approach to enhance different properties of the coatings (Ref 20-22). Recent progress regarding this strategy has been reviewed by Lu et al. (Ref 23). Many researchers studied the corrosion and wear behavior of PEO coatings on magnesium alloys (Ref 19, 24, 25). However, due to the relatively high porosity and limited range of phase compounds, these coatings are not capable to provide full maintenance under the long-term corrosion and wear conditions (Ref 21, 26, 27).

One of the most important recent issues regarding the PEO coatings is the in situ incorporation of solid particles into the coatings to improve the microstructure, phase composition and coating properties. Different particles were incorporated into PEO coatings on Mg alloys to improve their wear resistance (Ref 19). The addition of some particles with high self-lubricity properties into PEO coatings is reported to enhance the wear resistance of Mg alloys (Ref 20, 28). Particles such as PTFE (Polytetrafluoroethylene), graphite, MoS$_2$ were incorporated

Ebrahim Mortezanejad, Masoud Atapour, Hamidreza Salimijazi, Amir Alhaji, and **Amin Hakimizad**, Department of Materials Engineering, Isfahan University of Technology, 84156-83111 Isfahan, Iran. Contact e-mails: e.mortezanejad@gmail.com and m.atapour@cc.iut.ac.ir.

into the PEO coatings produced on titanium and aluminum alloys, but rarely for magnesium alloys (Ref 29-32). Mingo et al. (Ref 33) reported that the size and volume fraction of the reinforcing phase are two critical factors influencing the wear performance of the PEO coatings. Also, the hardness, thickness and compactness of the coatings are important factors affecting the wear resistance of the PEO coatings (Ref 27).

Recently, Davari et al. (Ref 34) focused on the multi-walled carbon nanotubes (MWCNTs)-reinforced PEO coating on AZ31B Mg alloy and reported that the addition of MWCNTs can lead to microstructural modifications and wear resistance improvements. In a similar work by Pezzato et al. (Ref 35), it has been reported that the graphite nanoparticles can improve the wear resistance of PEO coatings formed on AZ91 and AZ80 alloys. In another attempt, the effect of a sealing treatment in boiling water was investigated on the corrosion and mechanical aspects of the PEO coatings on AZ80 alloy and reported that the sealing treatment led to a remarkable improvement in the corrosion resistance (Ref 36). In situ incorporation of SiO_2, TiO_2 and Al_2O_3 nanoparticles into the aluminate-based PEO coatings has been explored to be an effective strategy to improve the wear resistance of the coating (Ref 24).

Incorporation of PTFE particles into PEO coatings on magnesium alloys has been investigated in the last decade for corrosion and were resistant applications. Due to low cost, high chemical stability and self-lubricating, PTFE particles were applied to improve the functionality of the PEO coatings (Ref 27). The non-uniform distribution of PTFE particles due to their high hydrophobicity and their low melting point (327 °C) is reported to be the most important challenges of using PTFE particles in PEO (Ref 27). Chen et al. (Ref 27) reported that the PEO coatings with PTFE can provide a very low friction coefficient (less than 0.1). In a similar work, it has been demonstrated that the PTFE-composite coatings fabricated on AM60B magnesium alloy are able to provide excellent lubrication and tribological properties (Ref 20).

As aforementioned, the fabrication of PTFE-incorporated coatings on Mg alloys is a novel approach to produce coatings with new functionalities. On the other hand, the kind of PEO electrolyte is a key factor to control different aspects of the coatings. The role of PTFE addition in enhancing the corrosion resistance and wear performance of the PEO coatings fabricated in different electrolytes can be an interesting and important work. In this work, a comparative study on the coatings produced in aluminate- and phosphate-based electrolytes containing PTFE nanoparticles has been conducted to investigate the role of electrolyte chemistry on the wear and corrosion of the coatings.

2. Experimental

2.1 Materials

In this study, the magnesium alloy AZ80 (8.2% Al, 0.6% Zn, 0.25% Mn, 0.03% Si, 0.003% Cu, 0.003% Fe and Mg balance) was used as substrate. For wear tests, disks with a diameter of 50 mm and a thickness of 6 mm, and for other tests, specimens with a diameter of 20 mm and thickness of 3 mm were prepared. Prior to the PEO coating process, the specimens were progressively ground with emery papers to 2400 grit, washed with ethanol and then dried.

2.2 PEO Process

To study the role of PTFE nanoparticles (200-300 nm), PEO treatment was performed in the aluminate- and phosphate-based electrolytes, as identified in Table 1. The x-ray diffraction pattern and the scanning electron microscopy (SEM) image of the PTFE particles are shown in Fig. 1(a) and (b), respectively. PEO process was conducted using a unipolar power supply at a constant current density of 5 A/dm^2 with the maximum voltage of 480 V for time duration of 10 min. The pulse frequency and duty cycle were fixed at 1 kHz and 10%, respectively. After the coating process, the specimens were washed with distilled water and then dried. Samples and stainless steel tubes were used as anode and cathode, respectively. The temperature of the electrolyte was kept at 25 ± 2 °C using a water cooling system. The pH values were varied from 12.2 to 12.3.

As you know, the agglomeration of nanoparticles is a popular phenomenon due to very high contact surface area of these particles. In this work, we have added sodium dodecyl sulfate anionic surfactant (0.5 g/l) in the electrolyte in order to prevent the agglomeration of the powders and also to make a stable dispersion of the particles. In the first step, 0.5 g/l of sodium dodecyl sulfate particles was dissolved in distilled water and then the PTFE nanoparticles were added to solution and a stable suspension was obtained by magnetic stirring for 30 min. The PEO coatings fabricated in aluminate and phosphate electrolytes without and with PTFE nanoparticles were named as A (aluminate), AP (aluminate + PTFE), P (phosphate) and PP (phosphate + PTFE).

2.3 Coating Characterization

The surface and cross section morphology of the coatings were evaluated using a scanning electron microscope (SEM, model Philips XL30) equipped with x-ray energy-dispersive spectroscope (EDS). The phase composition of the coatings was determined by an x-ray diffractometer (model Philips X'Pert-MDP) using Cu Kα radiation (λ = 0.15406 nm, 40 kV and 30 mA) in a grazing mode with a step size of 0.05°, in the range of 10-80°, and θ_s=3°. The infrared radiation (IR) examinations were performed using a Perkin Elmer Spectrum 2000 FTIR spectrometer with a wavelength range from 2500 to 16000 nm and a frequency of 1.9×10^{13} to 1.2×10^{14} Hz under dry air at room temperature.

2.4 Wear Test

The wear behavior of the coatings was evaluated using a pin-on-disk tribometer at 25 ± 2 °C. The coated specimens were allowed to slide against AISI52100 steel counterparts with a diameter of 6 mm at a speed of 0.1 m/s and a sliding distance of 500 m. The wear examinations were carried out under two loads of 3 N and 5 N. These loads were chosen based on the preliminary experiments and the published papers (Ref 37). The wear tracks and the worn pin surfaces were studied using SEM and energy-dispersive spectroscopy (EDS) analyses. To ensure repeatability, all tests were repeated for at least three times and the mean values were reported.

Table 1 The composition of the electrolytes used for PEO treatment

Electrolyte	Sample code	$NaAlO_2$, g/L	Na_3PO_4, g/L	KOH, g/L	PTFE, g/L
Aluminate without PTFE	A	10	…	2	…
Aluminate with PTFE	AP	10	…	2	10
Phosphate without PTFE	P	…	10	2	…
Phosphate with PTFE	PP	…	10	2	10
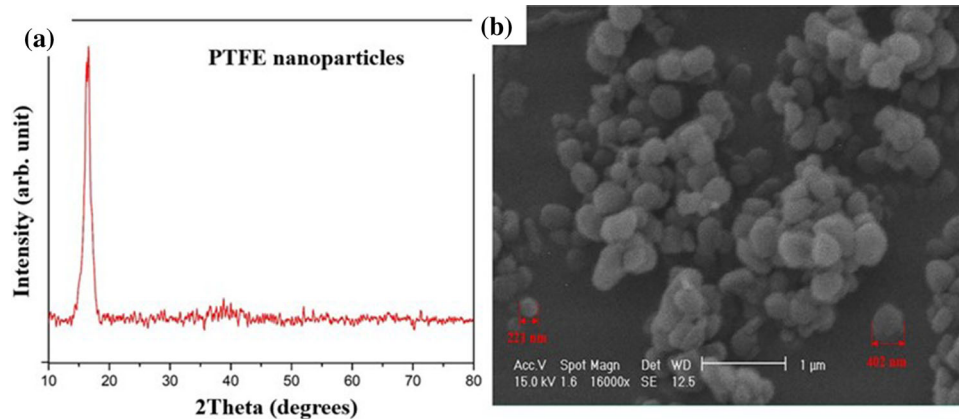
Fig. 1 (a) X-ray diffraction pattern and (b) SEM image of the used PTFE nanoparticles

2.5 Corrosion Test

The corrosion behavior of different coatings was evaluated in 0.5 wt.% NaCl solution using a computer-controlled potentiostate/galvanostate AMETEK system (PARSTAT 2237) at room temperature. A three-electrode cell including the coated sample (as working electrode with a contact surface of 0.5 cm^2), a counter electrode (platinum) and a reference electrode (Ag/AgCl saturated KCl electrode) was used. Potentiodynamic polarization experiments were carried out from 0.25 to + 0.6 V_{OCP} at a scanning rate of 0.5 mV/s. Corrosion parameters were obtained using the Tafel extrapolation method. Electrochemical impedance spectroscopy (EIS) tests were carried out at 100 kHz to 100 mHz and 10 mV peak-to-peak voltage amplitude after 4, 24, 48 and 72 h of immersion time. The EIS results were extracted and fitted using ZView software. All corrosion tests were repeated at least three times.

3. Results and Discussion

3.1 Voltage-Time Characteristic

Figure S_1 shows the time-voltage variation during PEO treatment in alumina- and phosphate-based electrolytes with and without PTFE nanoparticle. Very similar trend for two solutions was observed. However, the work and final voltage obtained for the coatings with PTFE nanoparticles were slightly smaller than that observed for the coatings prepared in particle-free electrolytes. It confirms that the addition of PTFE can affect the growth rate of the coatings. Furthermore, it can be seen that the breakdown potentials (E_{bd}) of coatings A and AP were less than that of coatings P and PP. In other words, the coating process in aluminate electrolyte was faster than that in phosphate electrolyte. Also, it is well known that increasing the conductivity of the electrolyte leads to decreasing of the final voltage (Ref 19). Conductivity of the electrolyte is one of the key factors affecting the growth rate of the coating. Higher conductivity of the electrolyte is associated with higher thickness of the coating. In this condition, the rate of film formation is more than the rate of anodic dissolution.

3.2 Microstructure

The SEM images of the coatings fabricated in the phosphate- and aluminate-based electrolytes with and without PTFE particles are shown in Fig. 2. The porous morphology for all coatings is due to the production of discharge channel and internal explosions of plasma bubbles during the PEO process. According to Fig. 2(a), the coating A exhibited high porosity but the addition of PTFE particles significantly reduced the size and the number of pores in the coating AP (Fig. 2b). This behavior can be attributed to the melting of PTFE and blocking the discharge channels during PEO treatment, which reduced the size and the number of pores. Similar behavior was reported for the beneficial role of CeO_2 (with the melting point of 2750 °C) in decreasing the porosity of PEO coatings (Ref 19). By comparison of the SEM images obtained from aluminate- and phosphate-based electrolytes, it can be deduced that the phosphate-based coatings exhibited fewer but larger pores. Also, it can be seen from Fig. 2(d) that the porous layer of the phosphate-based coating was strongly sealed by PTFE nanoparticles.

The distribution of PTFE nanoparticles in the coatings was investigated using EDS elemental mapping, and the results are presented in Fig. S_2. It confirms a uniform distribution of Mg, O and Al elements over the coating AP and a uniform distribution of Mg, O, and P elements over the PP coating. The presence of fluorine and carbon in the elemental maps of both
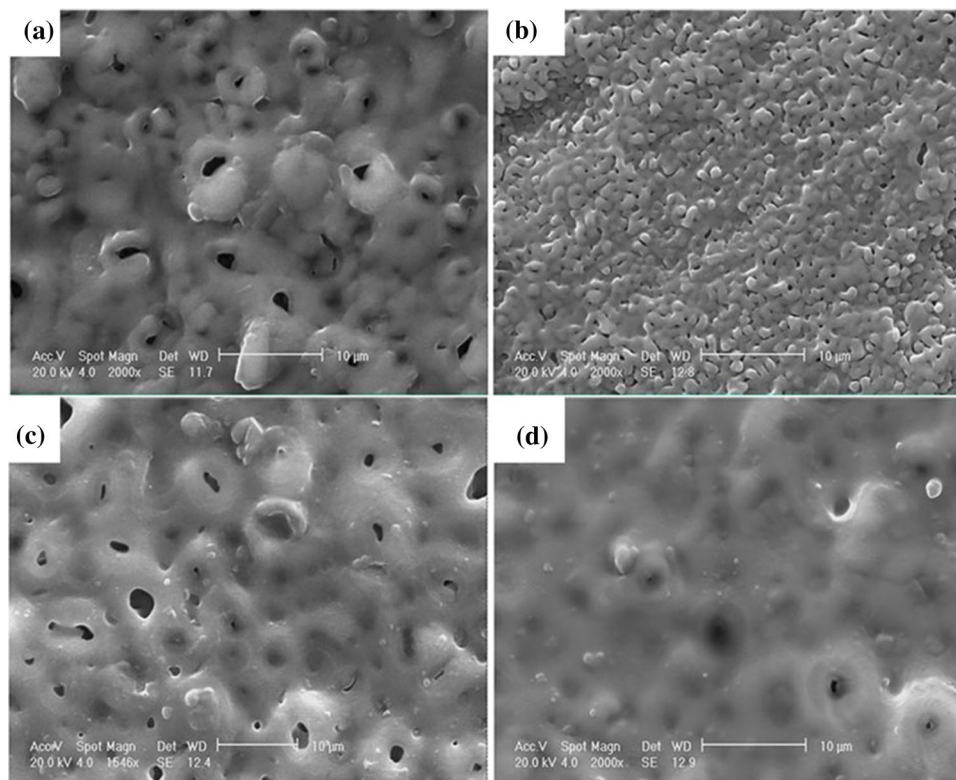
Fig. 2 SEM images of the surface of the coatings produced in different electrolytes with and without PTFE nanoparticles: (a) A, (b) AP, (c) P, (d) PP

Table 2 Roughness and thickness of the PEO coatings on AZ80 magnesium alloy

| Coating	R_z, μm	R_a, μm	Thickness, μm
A	22.08 ± 2.07	1.877 ± 0.05	19.14 ± 0.82
AP	21.14 ± 1.82	1.28 ± 0.29	20.43 ± 0.98
P	24.58 ± 1.14	2.64 ± 0.07	17.63 ± 0.58
PP	23.14 ± 1.19	2.11 ± 0.18	18.26 ± 0.36

coatings was related to the presence of PTFE nanoparticles in the coatings. It needs to mention that the only origin of fluorine in the coatings was electrolyte. As shown in the EDS map (Fig. S2), a high density of fluorine was observed around the pores. This showed that the PTFE nanoparticles were successfully incorporated in the pores.

The molten Mg formed due to the very high temperature associated with discharge phenomenon during PEO treatment converted to the magnesium oxide phases in the electrolyte (Ref 27, 38). The rapid cooling of magnesium oxides in contact with the electrolyte leads to the formation of pancake and volcanic craters structures (Ref 27). The coating prepared in aluminate electrolyte (Fig. 2a) exhibited a microstructure with high pancake-type morphology (a convex structure with an intermediate pore). In contrast, the phosphate-based coatings revealed volcanic-crater-type structure (Ref 24, 38). The results of the roughness measurements from five different points of the surfaces and the average thickness of coatings (obtained from ten areas) are presented in Table 2. It can be concluded that the thickness of the coating prepared in the aluminate electrolyte

was higher than that produced in the aluminate electrolyte. It can be related to the faster growth of the coating in aluminate electrolyte or decreased dissolution rate in this solution. A similar trend was observed by Cheng et al. (Ref 27) for PEO coatings fabricated in silicate- and aluminate-based electrolytes. Furthermore, the formation of the larger porosity in the surface of phosphate coating can be probably due to its high roughness. Also, some microcracks were formed in the coatings due to the presence of thermal stresses during the rapid freezing of the molten material. It needs to note that different plasma chemical reactions were conducted in both PEO electrolytes. It has been reported that different surface morphologies can be formed due to formation of different discharges during PEO (Ref 38, 39).

The values of R_a and a_z represent the average roughness and the mean distance from the highest peak to the deepest valley at the surfaces, respectively. From these results, it can be deduced that the average roughness of the coatings prepared in aluminate-based electrolytes was lower than that obtained in phosphate-based electrolyte. The higher roughness of the phosphate-based coatings can be attributed to their volcanic crater structure. It has been reported that the porosity and roughness can facilitate micrometric sources for storing lubricants and their continuous injection to the surfaces (Ref 27).

It can be seen from Fig. 3 that the addition of PTFE nanoparticles made a denser cross section structure and superior adhesion to the substrate. Since strong discharges occurred on the PTFE-free coatings and these discharges penetrated to the metal/coating interface, large porosities in the interface have been observed (Ref 27). Also, according to the cross-sectional images (Fig. 3), fine pores were formed due to the gas generated during the coating process and their trapping in the
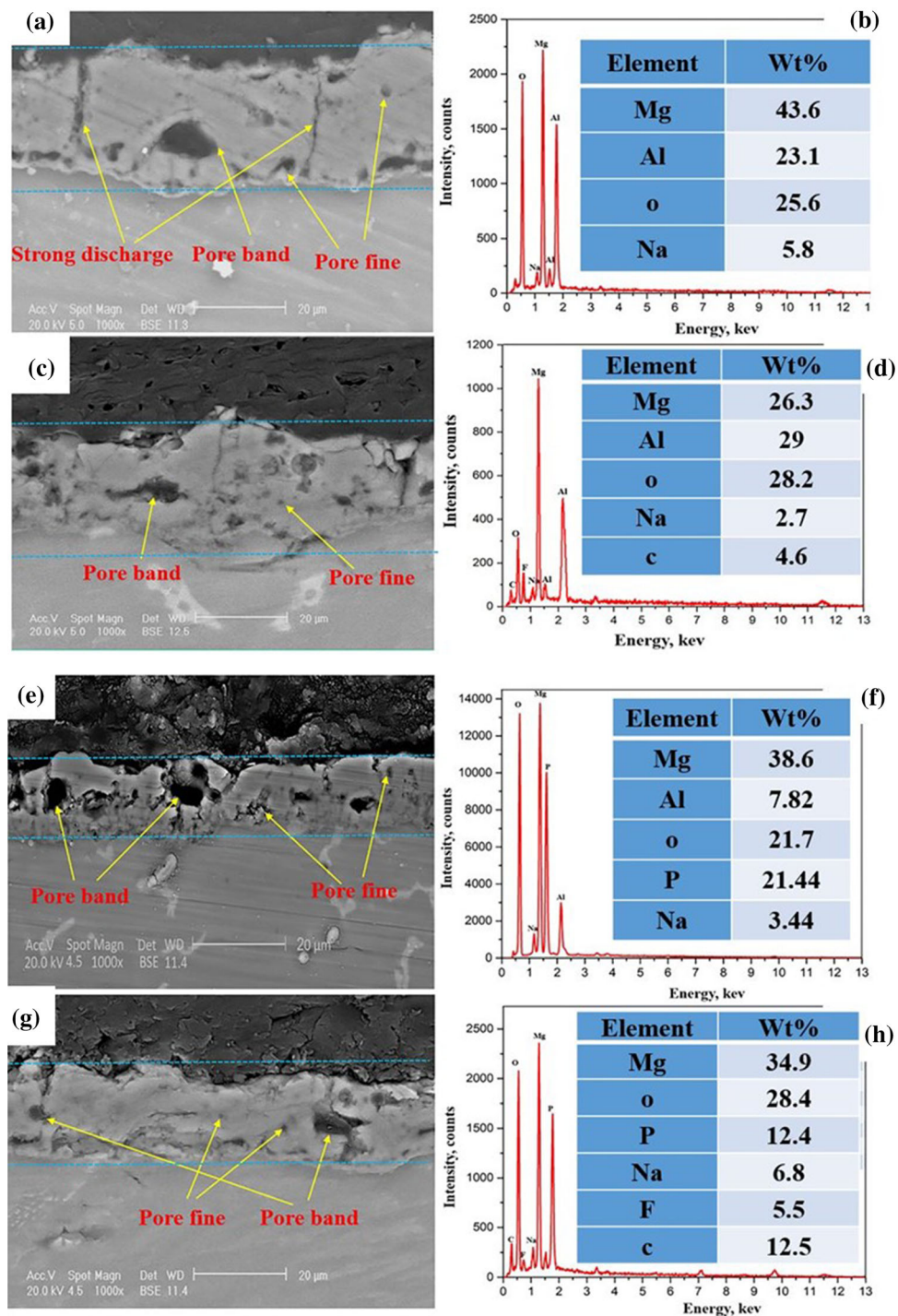
Fig. 3 SEM images and an elemental analysis of the cross sections of the coatings A (a, b), AP (c, d), P (e, f), PP (g, h)

coating structure (Ref 27). Because of the high viscosity of the electrolyte, the formation of small gas bubbles led to the formation of ridge-like protrusions on the surface of the coating (Ref 27). Also, it can be observed that the addition of PTFE led to the uneven appearance of the coatings (Ref 27). As shown in Fig. 3, the main constituents of both coatings A and AP were Mg, O and Al. However, high amounts of F and C elements were detected in the coating AP due to the presence of PTFE in this coating. Meanwhile, Mg, O and P were the main elements of P and PP coatings and F and C were found in the PP

coatings. It can be concluded that the nanoparticles were successfully introduced into the coating (because the only source of F was PTFE nanoparticles). The presence of F in the cross section of coatings AP and PP can be a valid reason for further sealing of the PEO coatings by PTFE particles. During the PEO coating process, PTFE nanoparticles with a negative zeta potential can move toward the anode (Mg alloy) and then deposit on the surface of the magnesium alloy (Ref 19). These particles can partially fill the pores and cracks of the PEO coatings (Ref 19).
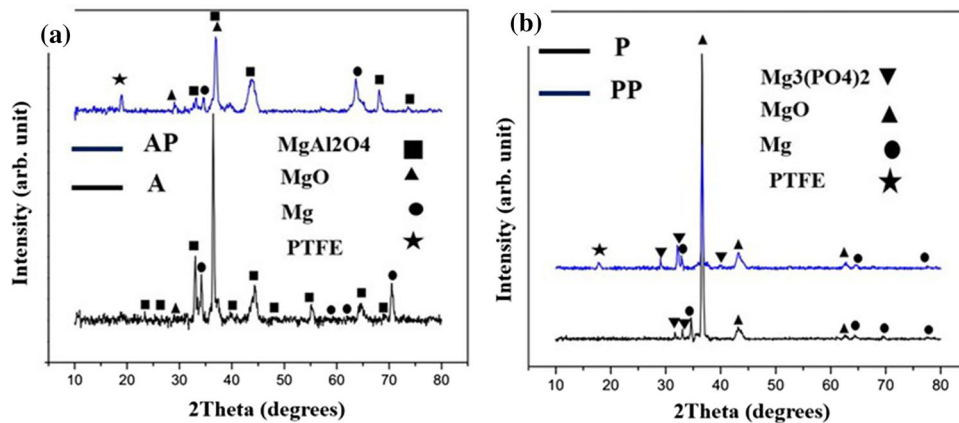
Fig. 4 The XRD patterns of different coatings (a) A and AP, (b) P and PP

Figure 4(a-b) shows the x-ray diffraction patterns obtained by grazing incidence method. These results confirmed that the aluminate-based coatings were mainly composed of MgO and MgAl$_2$O$_4$ phases. The phosphate-based coatings consisted of MgO and Mg$_3$PO$_4$ phases. It was clearly found that the intensity of the magnesium peaks decreased by adding PTFE particles to the electrolyte baths. The formation of MgAl$_2$O$_4$ phase can be ascribed to the reaction between Al$_2$O$_3$ and MgO at high temperatures (Ref 19, 40).

Fourier transform infrared spectroscopy (FTIR) was carried out to study the intermolecular bindings between the components of coatings. As shown in Fig. S$_3$, the peaks appearing at 1230 and 2850 cm^{-1} are related to the symmetric stretching bonds of C-F$_2$ and the peak at 1450 is pertained to the symmetrical bending bonds of C-F for the AP coating (Ref 41). In the case of the coating PP, the bonds at 1450, 1660, 1703 and 2850 cm^{-1} are assigned to the stretching bonds of C-F$_2$, stretching bonds of C-F, stretching bonds of C-O, and the wagging bonds of C-F$_2$, respectively (Ref 41, 42). These results indicated the presence of PTFE nanoparticles in the PEO coatings.

3.3 Wear Performance

3.3.1 Wear Behavior of Coatings under a Load of 3N. The wear behavior of all coated specimens was investigated using a pin-on-disk machine under 3 N and 5 N loads against AISI 52100 steel pins at room temperature. Figure 5 illustrates the friction coefficient of the coatings with and without PTFE nanoparticles. After about 100 m of sliding, the coatings A and P exhibited the friction coefficient values of 0.6 and 0.5, respectively. It means different wear behaviors occurred for different coatings. It can be seen that the coating prepared in the aluminate electrolyte revealed higher friction coefficient values than that obtained for the phosphate-based coating.

It has been reported that the occurrence of the three-body abrasive and the coating failures is the main wear mechanism of PEO coatings (Ref 19). The higher friction coefficient of the aluminate-based coating can be attributed to the occurrence of severe wear due to its higher roughness and porosity. Different friction coefficient values were recorded for the coatings with PTFE nanoparticles. In the case of coating PP, some sudden drops were observed in the first 50 m of sliding distance, which was due to localized failures and low loading capacity of the
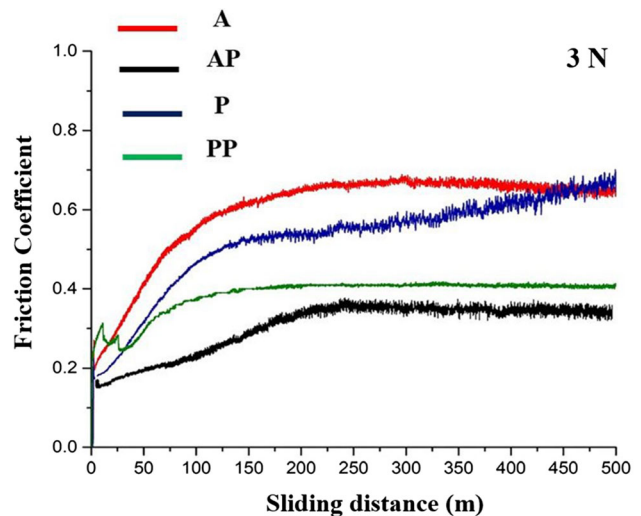

Fig. 5 Variation in friction coefficient with sliding distance for different coatings of A, P, AP and PP, under load of 3 N

Table 3 Friction coefficient of coatings under 3 N and 5 N loads

	Coating			
	A	P	AP	PP
3 N	0.64 ± 0.09	0.7 ± 0.11	0.33 ± 0.07	0.4 ± 0.05
5 N	0.2 ± 0.04	0.18 ± 0.05	0.33 ± 0.07	0.4 ± 0.06

coating (Ref 28). Also, some researchers reported that the sharp decrease in friction coefficient during the initial distances can be due to the destruction of the closed porosity and the formation of some solid lubricant between the coatings and their counterparts (Ref 27). The friction coefficient of the coating PP was about 0.4 in a steady-state condition. Among the tested coatings, the coating formed in the aluminate electrolyte in the presence of PTFE nanoparticles exhibited the lowest friction coefficient of 0.3 in steady-state condition. The results of the friction coefficient of coatings under the load of 3 and 5 N are presented in Table 3. It can be deduced that the

wear behavior of the PEO coatings strongly depends on their morphology and phase structure. It has been accepted that PTFE can decrease the friction coefficient by acting as a solid lubricant between the coating and the pin surfaces (Ref 28). However, the surface roughening of the pin caused by wear may promote the friction coefficient. Also, the formation of the hard debris or abrasive slurries trapped between moving surfaces is the another phenomenon that increased the friction coefficient. It has been reported that the three-body abrasive mechanism is the main mode of wear for PEO coatings (Ref 43). According to Fig. 5, during the first 100 m test under 3 N load, the friction coefficient of coating PP was increased to 0.6 and with the continuous wear test up to 280 m, the friction coefficient gradually tended to be stable (around 0.65). The occurrence of a small drop in the friction coefficient of coating PP after 280 m of sliding can be related to the coating failures. However, this coating was not completely removed after 500 m of sliding.

Figure 6 shows the wear tracks morphologies of different coated specimens after 500 m sliding distance. The worn tracks of the coatings fabricated in the two electrolytes without PTFE (Fig. 6a and d) reveal wider wear scar than that for the PTFE-containing coatings (Fig. 6c and d). The formation of deep parallel lines on the wear tracks of the coatings without PTFE demonstrated that severe wear mechanism was activated. Despite the deep wear lines on the surface of the coatings A and P, the destruction of these coatings did not completely occur. Because the thickness of the coatings A and P was 19.41 and 17.63 μm, respectively, while the wear depth of the coatings A and P was 13.78 and 14.26 μm, respectively. Furthermore, it can be seen that the phosphate coating (P) revealed shallower wear track than that of the aluminate coating (A). The SEM morphologies of these worn surfaces are consistent with the trends of friction coefficient of coatings.

The worn surfaces of the coatings (Fig. 6) revealed that the wear resistance of the PTFE-containing coatings is obviously enhanced, and the wear resistance of the coating AP was better than that of the coating PP (Fig. 6b and d). Superior wear resistance of coatings made in the PTFE-containing electrolytes (Fig. 6b and d) can be related to their high compression and sealing effect of the PTFE nanoparticles.

The SEM images of the worn steel pins surfaces slid against coatings under the 3 N load are presented in Fig. 7(a-d). The appearance of the worn pins revealed the occurrence of a mild wear mechanism. The wear debris are visible on the surface of all pins. However, the SEM images of the pin's surfaces show that the pin surfaces slide against coatings A and P (specimens without PTFE nanoparticles) exhibited the presence of more amount of wear debris compared to the pin surfaces slide against coatings AP and PP. It confirms that the addition of PTFE nanoparticles significantly improved the wear resistance of the coatings prepared in aluminate and phosphate electrolytes (Ref 27).

In fact, these particles reduced the direct contact between steel pin and the coatings and decreased the friction coefficient (Ref 27). The scanning electron micrograph of the wear tracks revealed that the surface of the steel counterpart was covered with transferred debris extracted from the coated specimens. It can be deduced that the adhesive wear mechanism was also activated after the initial abrasive mode surface of the steel pins.

3.3.2 Wear Behavior of Coatings under a Load of 5 N. The wear behavior of different coatings was examined at 5 N load, and the results of friction coefficients vs. sliding distance are shown in Fig. 8. The results of the friction coefficient of coatings under the load of 5 N are presented in Table 3. After about 100 m sliding, both coatings prepared in the absence of the PTFE (A and P) exhibited a constant friction coefficient of approximately 0.2, which was the friction
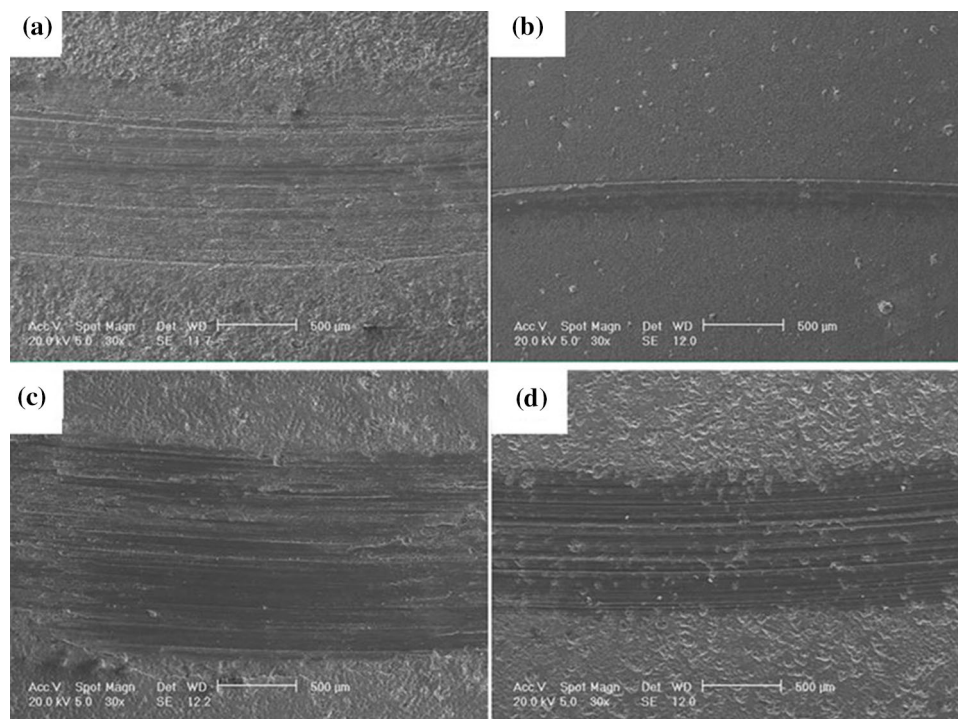
Fig. 6 SEM micrographs of wear track PEO coatings made in the presence and absence of PTFE particles. (a) A, (b) AP, (c) P and (d) PP
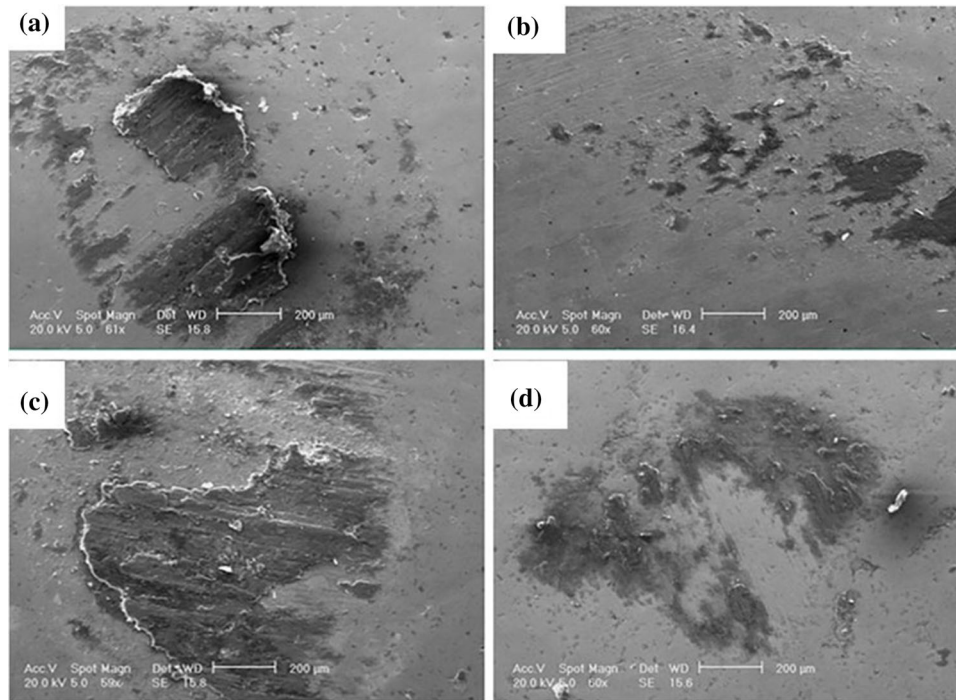
Fig. 7 SEM images showing surface of the steel pin counterparts slid against coated specimens under 3 N load on the coatings (a) A, (b) AP, (c) P, (d) PP
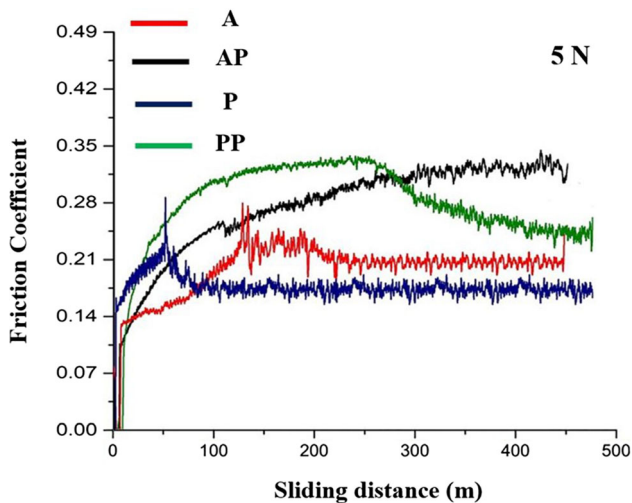
Fig. 8 Variation in friction coefficient vs. sliding distance for A, P, AP and PP coatings under 5 N load

coefficient of the uncoated base metal. It can be concluded that in the wear tests performed under 5 N load, both coatings A and P were completely broken and removed from the surface. However, both coatings AP and PP exhibited a superior wear resistance compared to the coatings A and P at 5 N load. A sudden drop in the friction coefficient of coating PP after around 300 m sliding can be related to the grinding away of the top layer. The coating AP was resistant against wear during the test.

The SEM images of the wear scars formed during the wear tests under load of 5 N are shown in Fig. 9. It can be seen that a severe abrasive wear was the prevailing mechanism of the

degradation of coatings A and P. However, in the case of the coatings AP and PP, the coating materials still remained after wear tests in the same conditions. For both coatings, removing the top layer has occurred. The coating AP revealed much lower wear compared to the coating PP. These results are in accordance with the friction coefficient behavior of coatings.

Figure 10 shows the SEM micrographs of steel pins slid against different coatings under the load of 5 N. The pins maintained their original spherical shape. It can be seen that the amount of wear debris was increased with increase in the load from 3 to 5 N. Furthermore, in all the conditions, the adhesion wear mechanism was activated. Chen et al. reported that PTFE-enriched ridge-like protrusions were the main reason for improving the PTFE-containing PEO coatings (Ref 27). It is worth mentioning that the brittle nature and the ability to modify the low plastic form of the PEO coatings make them more susceptible to the abrasive wear mechanism (Ref 19). Also, the formation of $MgAl_2O_4$ phase with a higher hardness in the coating AP can be another factor enhancing the wear resistance (Ref 19).

Figure 10(a-d) shows an SEM image of the surface of the steel pins used to test the wear under the load of 5 N on the coatings. Under 3 N load, there were some wear debris on the surface of all pins, but the amount of wear debris increased under the load of 5 N. It has also increased with increasing load of coating damage. In general, the PEO process is associated with the release of the gas (oxygen) (Ref 14, 27). Oxygen bubbles can be absorbed on the surface and divided into small and large microbubbles, thereby increasing the intensity of the electric field at the edge of the bubbles (Ref 27). The sintering of PTFE particles, topically on the surface of the coating, causes ridge-like protrusions on the surface of which PTFE particles are enclosed within them (Ref 27). During the wear test, these particles were transferred to the surface and therefore
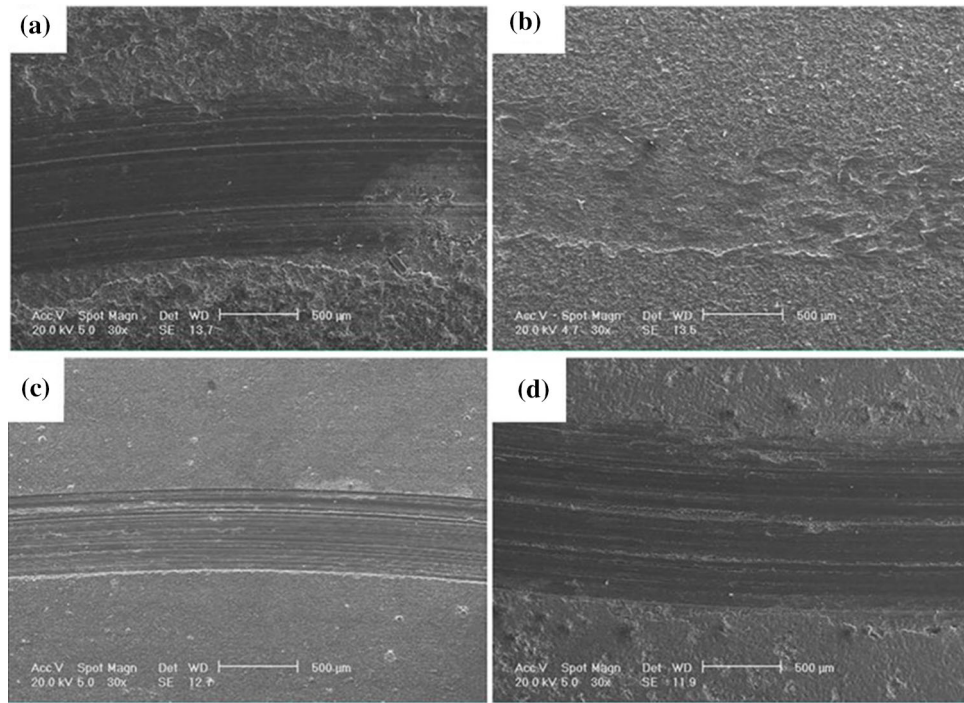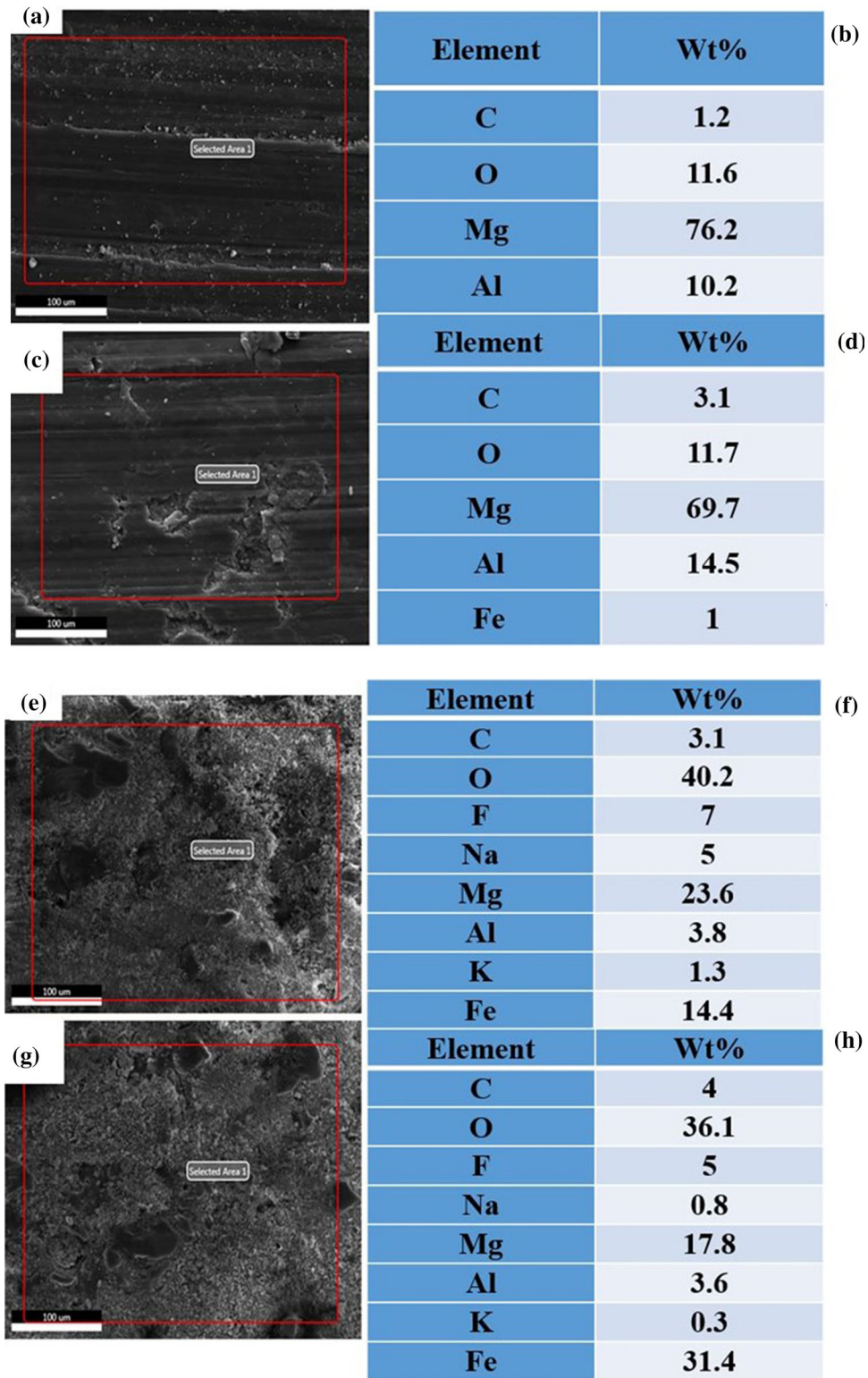
Fig. 9 SEM images showing surface of wear track PEO coatings made in the presence and absence of PTFE particles. (a) A, (b) AP, (c) P and (d) PP
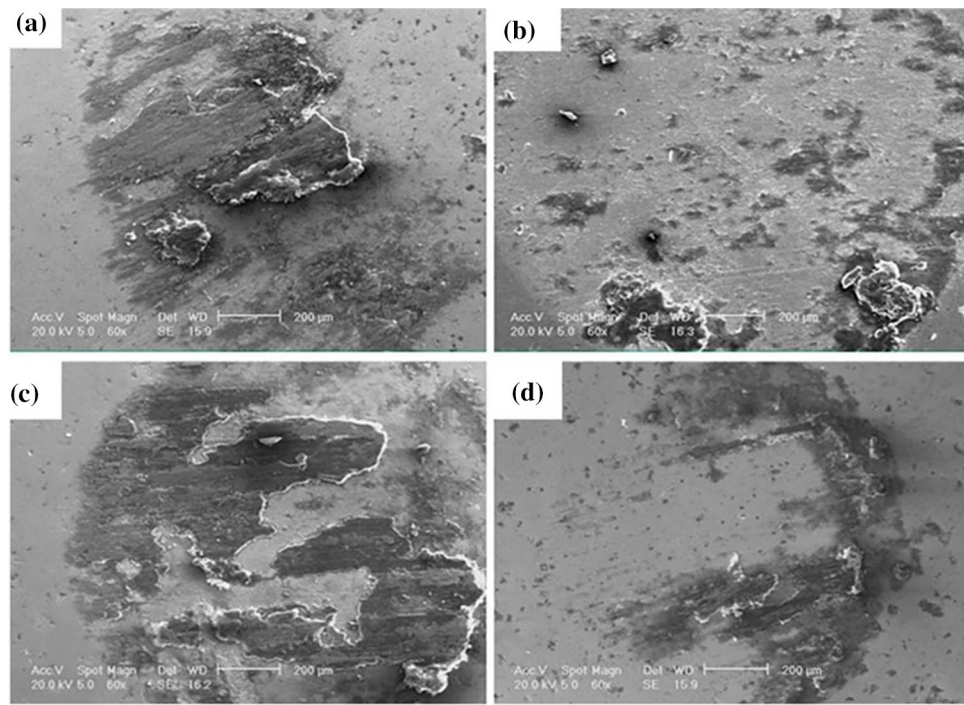
Fig. 10 SEM images showing surface of the steel pin counterparts slid against coated specimens under 5 N load on the coatings (a) A, (b) AP, (c) P, (d) PP

Element	Wt%
C	1.2
O	11.6
Mg	76.2
Al	10.2

Element	Wt%
C	3.1
O	11.7
Mg	69.7
Al	14.5
Fe	1

Element	Wt%
C	3.1
O	40.2
F	7
Na	5
Mg	23.6
Al	3.8
K	1.3
Fe	14.4

Element	Wt%
C	4
O	36.1
F	5
Na	0.8
Mg	17.8
Al	3.6
K	0.3
Fe	31.4

Fig. 11 High magnification SEM images and EDS results of different wear tracks after testing under 5 N load. (a) SEM micrograph of coating A, (b) EDS spectrum of the rectangle zone marked in (a), (c) SEM micrograph of coating P, (d) EDS spectrum of the zone marked in (c), (e) SEM micrograph of coating AP, (f) EDS spectrum of the zone marked in (e), (g) SEM micrograph of coating PP, (h) (d) EDS spectrum of the zone marked in (g)

acted as solid lubricants between the pin and the coating. This phenomenon reduced the coating degradation and COF (Ref 27). Also, the wear rate of coating AP was less than that of the coating PP due to the formation of the $MgAl_2O_4$ phase with a higher degree of hardness to the ceramic phase formed in the coating PP (Ref 19).

The wear mechanisms in light of both surface morphology and chemistry of the worn surfaces were identified. The SEM images and corresponding EDS analyses of the worn surface of coatings after sliding under 5 N load are presented in Fig. 11. As can be seen, the presence of the elements from the substrate (Mg, Al) in the worn surface of the coatings A and P confirmed the complete removal of these coating during wear experiments. In contrast, the worn surface of coatings AP and PP (Fig. 11 f and h) exhibited a high percentage of O and Mg, implying the presence of ceramic phases and a partial destruction of the coatings. Also, the presence of Fe in the EDS results of the wear track of these PTFE-containing coatings indicated that the wear process produced some damage in the steel pin.

3.4 Corrosion Studies

3.4.1 Potentiodynamic Polarization. Figure 12 shows the polarization curves of all coatings after 30 min immersion in 0.5 wt.% NaCl. The corrosion parameters are extracted from the polarization graphs and reported in Table 4. As can be seen, the addition of PTFE nanoparticles resulted in a significant improvement in corrosion performance of coatings. The
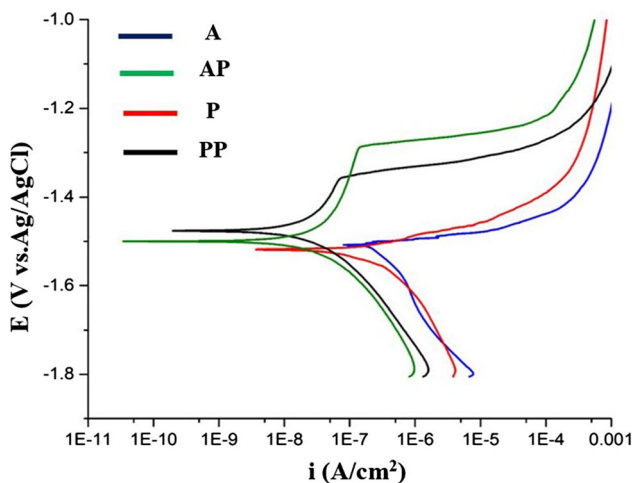

Fig. 12 Polarization curves of the coated samples after 30 min immersion in 0.5 wt% NaCl

corrosion potential (E_{corr}) was increased in positive direction, and the corrosion current density (i_{corr}) was significantly decreased by the addition of PTFE.

It has been reported that the corrosion performance of the PEO coatings mainly depends on the phases present, thickness and morphological aspects of the coatings (Ref 15). The superior corrosion resistance of phosphate coating can be related to its dense morphology with lower pore level. On the other hand, the relatively higher corrosion resistance of the aluminate-based coatings can be attributed to its higher porous surface morphology. As shown in Fig. 2, due to the relatively high porosity of PTFE-free coatings (A and P), the penetration of aggressive ions such as Cl⁻ into the porous layer increased the corrosion current density. It seems PTFE nanoparticles worked as an inhibitor during the immersion of coatings in a corrosive environment (Ref 28). Another point is that the breakdown potential (E_{bd}) of coatings A and P was close to the corrosion potential, while the coatings with PTFE particles (AP and PP) displayed a more positive E_{bd}. The E_{bd} of the composite coatings AP and PP was − 1278 and − 1322 mV, respectively, while the E_{bd} for coatings A and P was approximately equal to the corrosion potential. This behavior can be attributed to the increase in the compactness of the coatings with the addition of PTFE.

3.4.2 Electrochemical Impedance Spectroscopy. Electrochemical impedance spectroscopy (EIS) assessments were performed on the coatings after 4, 24, 48 and 72 h immersion in 0.5 wt.% NaCl solution. These immersion times were selected based on our preliminary tests and the literature (Ref 44-48). The Nyquist and bode-z diagrams for the coatings with and without PTFE are shown in Fig. 13(a-h). After assessment of different circuits and according to the previous studies (Ref 44), a two time constants equivalent circuit was used for fitting the EIS data (Fig. 13i). In these circuits, R_S is the unbalanced resistor, ($CPE_{out} − R_{out}$) is the time constant at high frequencies of the outer porous layer, and ($CPE_{in} − R_{in}$) is time constant at low frequencies (representing the internal barrier layer) (Ref 44).

According to the Nyquist diagrams, it can be deduced that the coatings exhibited a capacitive loop at high frequencies (10^2-10^5 Hz), relating to the outer porous layer with a low resistivity (Ref 26). A loop at low frequencies (0.01-10 Hz) was corresponding to the formation of an inner dense layer (with higher impedance than the outer porous layer) (Ref 49). According to the cross-sectional images of the coatings (Fig. 3), it was observed that in the presence of PTFE particles, large and continuous porosity was reduced in the metal/coating interface and the inner layer structure was relatively denser, thus penetrating destructive ions such as chloride through the
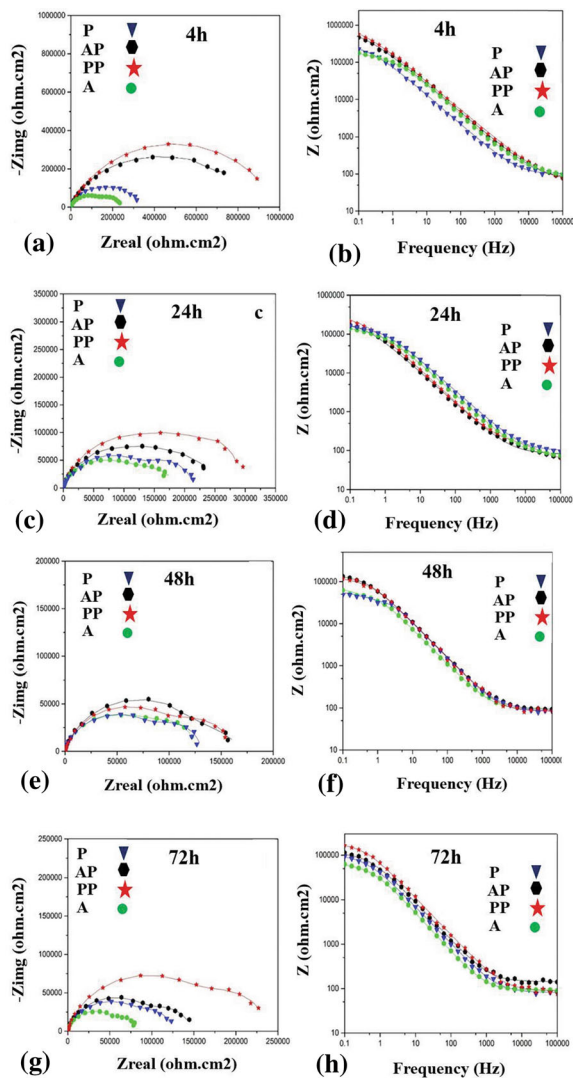
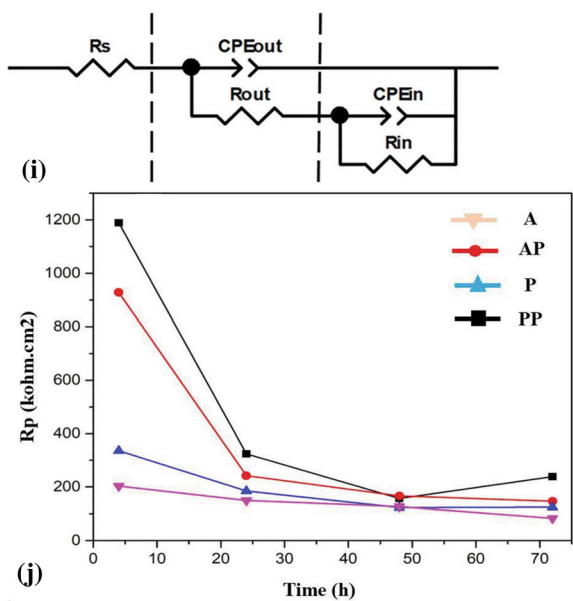**Table 4 Corrosion results of different coated samples after 30 min immersion in 0.5% NaCl**

Coating	E_{corr}, mV vs. Ag/AgCl	i_{corr}, nA/cm²	β_a, V/dec	β_c, V/dec
A	− 1520 ± 19	878.82 ± 3.2	0.027	0.232
P	− 1540 ± 27	644.91 ± 1.2	0.023	0.052
AP	− 1510 ± 31	161.82 ± 2.8	0.126	0.076
PP	− 1470 ± 18	84.71 ± 3.6	0.087	0.034

porous porosity, And reaching the substrate is delayed, thus improving the corrosion protection performance of the coating (Ref 50).

The variation in the total resistance of the inner barrier layer and the outer porous layer (Rp) with the immersion time is plotted in Fig. 13j. For all diagrams up to 24 h of immersion, the rate of resistance decrease is very high as the rate of penetration of corrosive ions into the coating is higher in the early times. The decrease in resistance at early immersion times is due to high defects such as micro-porosity and microcracks and greater surface area of contact with the electrolyte (Ref 26). Because in early times, the dissolution rate of the surface is higher and increases the inner surface of the porosity and cracks. Thus, in the 24-48 h time frame, the rate of resistance decline is much slower and even after 48 h, the trend of resistance increase is observed. The reason for this increase is due to the penetration of corrosion products into porosity and cracks (Ref 51).

SEM images of the surface of the coatings after 72 h of immersion in the corrosive solution are shown in Fig. 14. In Fig. 14(a) (coating A), a very large cavity is formed, probably based on EIS data to reach the substrate. However, for the AP coating, the degradation depth of the coating is lower, due to the decrease in the number and size of the porosity and thus the rate of penetration of corrosive ions into the coating. For coatings P and PP, the amount of degradation and depth is much lower than that for aluminate coatings. All these observations are consistent with data obtained from the EIS test. Therefore, it can be concluded that the presence of PTFE particles improves the corrosion resistance behavior of the coatings in both aluminate and phosphate electrolytes.

4. Conclusions

The effect of adding PTFE nanoparticles on the corrosion and wear behavior of aluminate- and phosphate-based PEO coatings on AZ80 magnesium alloy was investigated. The following main conclusions were drawn:

1. The results of the SEM examinations of the surface and cross section of the coatings showed that the nanoparticles were distributed uniformly throughout the coatings. Also, the incorporation of PTFE nanoparticles reduced the porosity and roughness of the coatings and improved the hardness.
2. For coatings containing nanoparticles, the appearance of a peak at an angle of 17 ° confirmed the successful penetration of the PTFE particles into the coatings. Also,
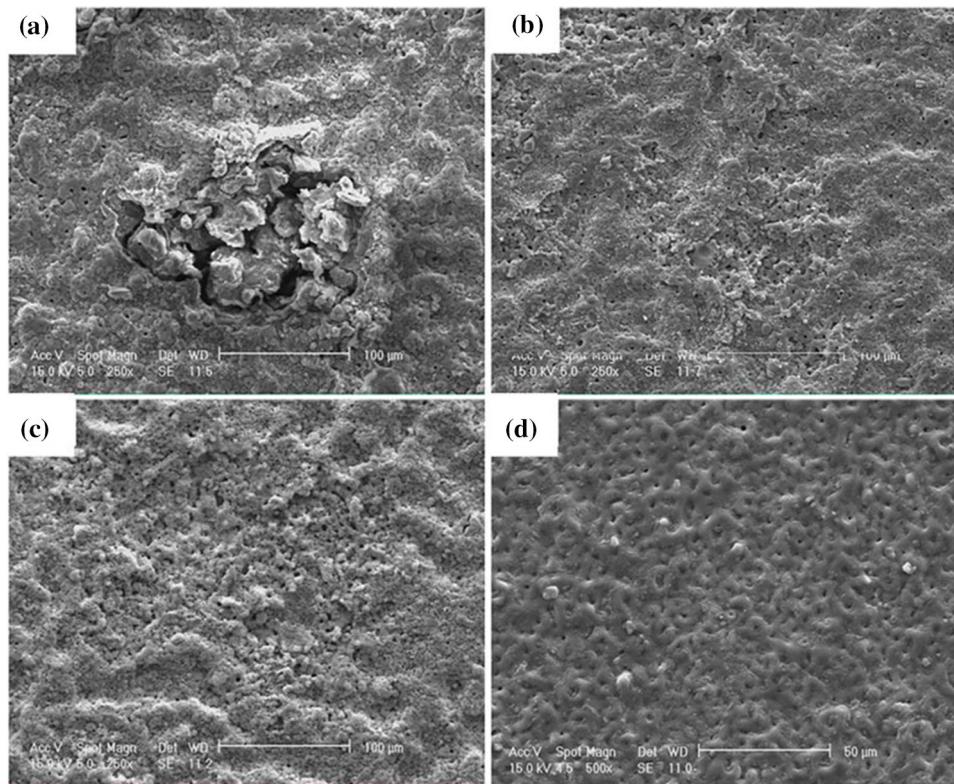
Fig. 14 SEM images of the surface of the coatings after 72 h immersion in 0.5 wt.% NaCl solution

FTIR analyses of the coatings showed that carbon-fluorine bonds were formed in the range of 500 to 400 cm^{-1}. Therefore, this confirmed the successful formation of PEO/PTFE nanocomposite coatings.

3. According to the wear evaluations under 3 N, the coatings with PTFE exhibited a low friction coefficient of 0.33 and 0.4 for the aluminate- and phosphate-based coatings, respectively. These friction coefficients were almost half of the values for the PTFE-free coatings.

4. Under the load of 5 N, the coatings without PTFE were completely removed but the nanocomposite coatings exhibited a very good wear resistance. Among the four coatings, the PTFE nanocomposite coating made at aluminate electrolyte showed the best wear resistance on account of its better compactness.

5. The corrosion examinations revealed that the PTFE addition improved the corrosion resistance of both PEO coatings produced at aluminate and phosphate electrolytes. This performance was related to the reduction in porosity and microcracks in PTFE nanocomposite coatings. Also, it was found that the addition of PTFE in aluminate coatings was more effective in improving the corrosion resistance of AZ80 than the PEO coating produced at phosphate electrolyte.

6. According to the EIS results after different immersion times (4, 24, 48 and 72 h), the PTFE nanocomposite coatings exhibited a superior corrosion resistance for all immersion times.

References

1. L. Tonelli, L. Pezzato, P. Dolcet, M. Dabalà and C. Martini, Effects of Graphite nano-Particle Additions on Dry Sliding Behaviour of Plasma-Electrolytic-Oxidation-Treated EV31A Magnesium Alloy Against Steel in Air, *Wear*, 2018, **404**, p 122–132

2. M. Daroonparvar, M.A.M. Yajid, N.M. Yusof and H.R. Bakhsheshi-Rad, Preparation and Corrosion Resistance of a nAnocomposite Plasma Electrolytic Oxidation Coating on Mg-1%Ca Alloy Formed in Aluminate Electrolyte Containing Titania Nano-Additives, *J. Alloys Compd.*, 2016, **688**, p 841–857

3. M. Ali, M.A. Hussein and N. Al-Aqeeli, Magnesium-Based Composites and Alloys for Medical Applications: A Review of Mechanical and Corrosion Properties, *J. Alloys Compd.*, 2019, **792**, p 1162–1190

4. J.E. Gray and B. Luan, Protective Coatings on Magnesium and its Alloys: a Critical Review, *J. Alloys Compd.*, 2002, **336**(1–2), p 88–113

5. H. Nasiri Vatan, R. Ebrahimi-Kahrizsangi and M. Kasiri-Asgarani, *Structural, Tribological and Electrochemical Behavior of SiC Nanocomposite Oxide Coatings Fabricated by Plasma Electrolytic Oxidation (PEO) on AZ31 Magnesium Alloy*, Elsevier, Amsterdam, 2016, p 241–255

6. N. Eslamzadeh, R. Ebrahimi-kahrizsangi, S. Karbasi, A. Zarebidaki and F. Gharavi, An Investigation into the Corrosion Behavior of MgO/ZrO$_2$ Nanocomposite Coatings Prepared by Plasma Electrolytic Oxidation on the AZ91 Magnesium Alloy, *J. Mater. Eng. Perform.*, 2017, **26**(9), p 4255–4264

7. R. Arrabal, A. Pardo, M.C. Merino, M. Mohedano, P. Casajús, E. Matykina, P. Skeldon and G.E. Thompson, Corrosion Behaviour of a Magnesium Matrix Composite with a Silicate Plasma Electrolytic Oxidation Coating, *Corros. Sci.*, 2010, **52**(11), p 3738–3749

8. D.V. Mashtalyar, S.V. Gnedenkov, S.L. Sinebryukhov, I.M. Imshinetskiy, A.S. Gnedenkov and V.M. Bouznik, Composite Coatings Formed Using Plasma Electrolytic Oxidation and Fluoroparaffin Materials, *J. Alloys Compd.*, 2018, **767**, p 353–360

9. W. Tu, Y. Cheng, X. Wang, T. Zhan, J. Han and Y. Cheng, Plasma Electrolytic Oxidation of AZ31 Magnesium Alloy in Aluminate-Tungstate Electrolytes and the Coating Formation Mechanism, *J. Alloys Compd.*, 2017, **725**, p 199–216

10. P. Bala Srinivasan, C. Blawert, M. Störmer and W. Dietzel, Characterisation of Tribological and Corrosion Behaviour of Plasma Electrolytic Oxidation Coated AM50 Magnesium Alloy, *Surf. Eng.*, 2010, **26**(5), p 340–346

11. Z. Yang, X.Z. Zhang, Y.K. Wu, D.D. Wang, X.T. Liu, G.R. Wu, P. Nash and D. Shen, Plasma Electrolytic Oxidation Ceramic Coatings Proceed by Porous Anodic Film, *J. Alloys Compd.*, 2020, **812**, p 152098

12. G. Li, Y. Mao, Z. Li, L. Wang and H. Dacosta, Tribological and Corrosion Properties of Coatings Produced by Plasma Electrolytic Oxidation on the ZA27 Alloy, *J. Mater. Eng. Perform.*, 2017, **27**(5), p 2298–2305

13. C. Blawert, S.P. Sah, N. Scharnagl and M.B. Kannan, Plasma Electrolytic Oxidation/Micro-arc Oxidation of Magnesium and Its Alloys, *Surf. Modif. Magnes. Alloy Biomed. Appl.*, 2015 https://doi.org/10.1016/B978-1-78242-078-1.00008-6

14. G.B. Darband, M. Aliofkhazraei, P. Hamghalam and N. Valizade, Plasma Electrolytic Oxidation of Magnesium and its Alloys: Mechanism, Properties and Applications, *J. Magnes. Alloy.*, 2017, **5**(1), p 74–132

15. V. Dehnavi, D.W. Shoesmith, B.L. Luan, M. Yari, X.Y. Liu and S. Rohani, Corrosion Properties of Plasma Electrolytic Oxidation Coatings on an Aluminium Alloy: the Effect of the PEO Process Stage, *Mater. Chem. Phys.*, 2015, **161**, p 49–58

16. E. Ziyaei, M. Atapour, H. Edris and A. Hakimizad, Corrosion Behavior of PEO Coatings Formed on AZ31 Alloy in Phosphate-Based Electrolytes with Calcium Acetate Additive, *J. Mater. Eng. Perform.*, 2017, **26**(7), p 3204–3215

17. A. Heydarian, M. Atapour, A. Hakimizad and K. Raeissi, The Effects of Anodic Amplitude and Waveform of Applied Voltage on Characterization and Corrosion Performance of the Coatings Grown by Plasma Electrolytic Oxidation on AZ91 Mg Alloy from an Aluminate Bath, *Surf. Coat. Technol.*, 2020, **383**, p 125235

18. Y. Mori, A. Koshi, J. Liao, H. Asoh and S. Ono, Characteristics and Corrosion Resistance of Plasma Electrolytic Oxidation Coatings on AZ31B Mg Alloy Formed in Phosphate: Silicate Mixture Electrolytes, *Corros. Sci.*, 2014, **88**, p 254–262

19. M. Atapour, C. Blawert and M.L. Zheludkevich, The Wear Characteristics of CeO$_2$ Containing Nanocomposite Coating Made by Aluminate-based PEO on AM50 Magnesium Alloy, *Surf. Coat. Technol.*, 2019, **357**, p 626–637

20. Z. Wang, L. Wu, Y. Qi, W. Cai and Z. Jiang, Self-Lubricating Al2O3/PTFE Composite Coating Formation on Surface of Aluminium Alloy, *Surf. Coat. Technol.*, 2010, **204**(20), p 3315–3318

21. X. Lu, M. Mohedano, C. Blawert, E. Matykina, R. Arrabal, K.U. Kainer and M.L. Zheludkevich, Plasma Electrolytic Oxidation Coatings with Particle Additions: a Review, *Surf. Coat. Technol.*, 2016, **307**, p 1165–1182

22. Z. Yao, Y. Xu, Y. Liu, D. Wang, Z. Jiang and F. Wang, Structure and Corrosion Resistance of ZrO2 Ceramic Coatings on AZ91D Mg Alloys by Plasma Electrolytic Oxidation, *J. Alloys Compd.*, 2011, **509**(33), p 8469–8474

23. X. Lu, C. Blawert, Y. Huang, H. Ovri, M.L. Zheludkevich and K.U. Kainer, Plasma Electrolytic Oxidation Coatings on Mg Alloy with Addition of SiO$_2$ Particles, *Electrochim. Acta.*, 2016, **187**, p 20–33

24. M. Shokouhfar and S.R. Allahkaram, Effect of Incorporation of Nanoparticles with Different Composition on Wear and Corrosion Behavior of Ceramic Coatings Developed on Pure Titanium by Micro Arc Oxidation, *Surf. Coat. Technol.*, 2017, **309**, p 767–778

25. M. Toorani, M. Aliofkhazraei and R. Naderi, Ceria-Embedded MAO Process as Pretreatment for Corrosion Protection of Epoxy Films Applied on AZ31-Magnesium Alloy, *J. Alloys Compd.*, 2019, **785**, p 669–683

26. J. Liang, P.B. Srinivasan, C. Blawert and W. Dietzel, Comparison of Electrochemical Corrosion Behaviour of MgO and ZrO2 Coatings on AM50 Magnesium Alloy Formed by Plasma Electrolytic Oxidation, *Corros. Sci.*, 2009, **51**(10), p 2483–2492

27. Y. Chen, X. Lu, C. Blawert, M.L. Zheludkevich, T. Zhang and F. Wang, Formation of Self-lubricating PEO Coating via in-situ Incorporation of PTFE Particles, *Surf. Coat. Technol.*, 2018, **337**, p 379–388

28. J. Guo, L. Wang, S.C. Wang, J. Liang, Q. Xue and F. Yan, Preparation and Performance of a Novel Multifunctional Plasma Electrolytic Oxidation Composite Coating Formed on Magnesium Alloy, *J. Mater. Sci.*, 2009, **44**(8), p 1998–2006

29. S. Ikonopisov, Theory of Electrical Breakdown During Formation of Barrier Anodic Films, *Electrochim. Acta.*, 1997, **22**(10), p 1077–1082

30. M. Hyung, J. Ju, S. Jin and H. Jang, Tribological Properties of Solid Lubricants (graphite, Sb 2 S 3, MoS 2) for Automotive Brake Friction Materials, *Wear*, 2006, **260**(7–8), p 855–860

31. B.S. Lou, J.W. Lee, C.M. Tseng, Y.Y. Lin and C.A. Yen, Mechanical Property and Corrosion Resistance Evaluation of AZ31 Magnesium Alloys by Plasma Electrolytic Oxidation Treatment: Effect of MoS2 Particle Addition, *Surf. Coat. Technol.*, 2018, **350**, p 813–822

32. J.S. Rudas, J.M. Meza, H.A. Estupin, J.S. Rudas, H.A. Estupin and J.M. Meza, Mechanical and Corrosion Behavior of Plasma Electrolytic Oxidation Coatings on AZ31B Mg Alloy Reinforced with Multiwalled Carbon Nanotubes, *J. Mater. Eng. Perform.*, 2020, **29**(2), p 1135–1145

33. B. Mingo, R. Arrabal, M. Mohedano, A. Pardo and E. Matykina, Corrosion and Wear of PEO Coated AZ91/SiC Composites, *Surf. Coat. Technol.*, 2017, **309**, p 1023–1032

34. M. Daavari, M. Atapour, M. Mohedano, R. Arrabal, E. Matykina and A. Taherizadeh, Biotribology and Biocorrosion of MWCNTs-Reinforced PEO Coating on AZ31B Mg Alloy, *Surf. Interface*, 2020, **22**, p 10085

35. L. Pezzato, V. Angelini, K. Brunelli, C. Martini and M. Dabala, Tribological and Corrosion Behavior of PEO Coatings with Graphite Nanoparticles on AZ91 and AZ80 Magnesium Alloys, *Trans. Nonferrous Met. Soc. China*, 2018, **28**(2), p 259–272

36. L. Pezzato, L.B. Coelho, R. Bertolini, A.G. Settimi, K. Brunelli, M. Olivier and M. Dabalà, Corrosion and Mechanical Properties of Plasma Electrolytic Oxidation-Coated AZ80 Magnesium Alloy, *Mater. Corros.*, 2019, **70**(11), p 2103–2112

37. M. Atapour, C. Blawert and M.L. Zheludkevich, The Wear Characteristics of CeO$_2$ Containing Nanocomposite Coating Made by Aluminate-based PEO on AM50 Magnesium Alloy, *Surf. Coat. Technol.*, 2019, **357**, p 626–637

38. R.O. Hussein, X. Nie and D.O. Northwood, An Investigation of Ceramic Coating Growth Mechanisms in Plasma Electrolytic Oxidation (PEO) Processing, *Electrochim. Acta.*, 2013, **112**, p 111–119

39. M. El-Dairi, R.J. House, Optic Nerve Hypoplasia, Handb. Pediatr. Retin. J. Mol. Struct. 285–287 (2019)

40. M. Sieber, F. Simchen, I. Scharf and T. Lampke, Formation of a Spinel Coating on AZ31 Magnesium Alloy by Plasma Electrolytic Oxidation, *J. Mater. Eng. Perform.*, 2016, **25**(3), p 1157–1162

41. C.Y. Liang and S. Krimm, Infrared Spectra of High Polymers: III—Polytetrafluoroethylene and Polychlorotrifluoroethylene, *J. Chem. Phys.*, 1956, **25**(3), p 563–571

42. R.H. Zhang, J. Zhao and J. Liang, A Novel Multifunctional PTFE/PEO Composite Coating Prepared by One-step Method, *Surf. Coat. Technol.*, 2016, **299**, p 90–95

43. A. Nominé, J. Martin, G. Henrion and T. Belmonte, Effect of Cathodic Micro-discharges on Oxide Growth during Plasma Electrolytic Oxidation (PEO), *Surf. Coat. Technol.*, 2015, **269**, p 131–137

44. J. Liang, P.B. Srinivasan, C. Blawert, M. Störmer and W. Dietzel, Electrochemical Corrosion Behaviour of Plasma Electrolytic Oxidation Coatings on AM50 Magnesium Alloy Formed in Silicate and Phosphate Based Electrolytes, *Electrochim. Acta.*, 2009, **54**(14), p 3842–3850

45. M.A. Chen, Y.C. Ou, C.Y. Yu, C. Xiao and S.Y. Liu, Corrosion Performance of Epoxy/BTESPT/MAO Coating on AZ31 Alloy, *Surf. Eng.*, 2016, **32**(1), p 38–46

46. Z. Li, X. Jing, Y. Yuan and M. Zhang, Composite Coatings on a Mg-Li Alloy Prepared by Combined Plasma Electrolytic Oxidation and Sol-gel Techniques, *Corros. Sci.*, 2012, **63**, p 358–366

47. M. Sun, A. Yerokhin, M.Y. Bychkova, D.V. Shtansky, E.A. Levashov and A. Matthews, Self-healing Plasma Electrolytic Oxidation Coatings Doped with Benzotriazole Loaded Halloysite Nanotubes on AM50 Magnesium Alloy, *Corros. Sci.*, 2016, **111**, p 753–769

48. M. Alaei, M. Atapour and S. Labbaf, Progress in Organic Coatings Electrophoretic Deposition of Chitosan-Bioactive Glass Nanocomposite Coatings on AZ91 Mg Alloy for Biomedical Applications, *Prog. Org. Coatings.*, 2020, **147**, p 105803

49. W. Shang, B. Chen, X. Shi, Y. Chen and X. Xiao, Electrochemical Corrosion Behavior of Composite MAO/sol-gel Coatings on Magnesium Alloy AZ91D using Combined Micro-arc Oxidation and Sol-gel Technique, *J. Alloys Compd.*, 2009, **474**(1–2), p 541–545

50. D.Y. Hwang, Y.M. Kim, D.Y. Park, B. Yoo and D.H. Shin, Corrosion Resistance of Oxide Layers Formed on AZ91 Mg Alloy in KMnO4 Electrolyte by Plasma Electrolytic Oxidation, *Electrochim. Acta.*, 2009, **54**(23), p 5479–5485

51. H. Duan, K. Du, C. Yan and F. Wang, Electrochemical Corrosion Behavior of Composite Coatings of Sealed MAO Film on Magnesium Alloy AZ91D, *Electrochim. Acta.*, 2006, **51**(14), p 2898–2908